sustainability

MDPI

Article

Advances in the Rheology of Synthetic Binder for Sustainable Road Pavements: An Improved Protocol for DSR Testing

Marco Pasetto, Andrea Baliello *, Giovanni Giacomello and Emiliano Pasquini

Department of Civil, Environmental and Architectural Engineering, University of Padova, Via Marzolo 9, 35131 Padova, Italy

* Correspondence: andrea.baliello@unipd.it

Abstract: Bituminous binders are thermal-dependent visco-elastic materials commonly used in pavement engineering. However, synthetic binders represent quite a new family of products that can be used in the substitution of conventional binders with various purposes. Among them, clear synthetic resins recently experienced a quick diffusion since they can be employed in the production of sustainable road pavements (which address aesthetic concerns, thermal aspects, etc.). Since specific studies addressing the rheological modeling of clear synthetic binders cannot be found in the literature, the purpose of this research is setting up an advanced rheological protocol to characterize such materials, bridging the existing knowledge gap. An extensive laboratory investigation with the dynamic shear rheometer was carried out in oscillatory mode (amplitude and frequency sweeps) to analyze the stress–strain state of such binders. An innovative test at a constant strain rate was used to construct non-linear master curves, overcoming various criticisms about the stress state of the binder when subjected to time-dependent deformations. Results indicated that, using non-linear data, horizontal and vertical shift factors (functions of temperature and strain rate) can be modeled through power law equations to obtain the master curves. This method was considered suitable for depicting the rheological response of the binders displaying such complex behaviors.

Keywords: synthetic binder; dynamic shear rheometer; non-linear testing; master curve; sustainable road pavement

Citation: Pasetto, M.; Baliello, A.; Giacomello, G.; Pasquini, E. Advances in the Rheology of Synthetic Binder for Sustainable Road Pavements: An Improved Protocol for DSR Testing. *Sustainability* **2023**, *15*, 5146. https://doi.org/10.3390/su15065146

Academic Editor: Liseane Padilha Thives

Received: 21 February 2023
Revised: 9 March 2023
Accepted: 10 March 2023
Published: 14 March 2023

1. Introduction

Bituminous binder is a thermal-dependent visco-elastic material on the rise in the design of bituminous mixtures for road pavement layers. Over the past years, its mechanical response under several conditions has been studied worldwide, with recent advances in the characterization of its rheological behavior being achieved through the greater capabilities of newer testing methods, equipment and protocols. As a consequence, several current studies are being carried out in view of the potential of laboratory simulations [1], which grant the reproduction of variable real-scale aspects [2] linked to road composition, traffic volumes, vehicle speeds [3] and environmental conditions [4]. This fact is promoted by a certain ease of testing, since it is widely known that bitumen assumes a linear visco-elastic behavior if subjected to low stress–strain levels [5].

In recent years, innovative binders with different natures have started to be used as alternatives in the manufacture of flexible pavements, becoming attractive thanks to optimized rheological behaviors (lower susceptibility to temperature, higher fatigue resistance, reduced rutting potential, etc.). As an example, actual interest by business and academic sectors has started to be directed toward bio-binders [6], chemical modified binders [7] and thermochromic asphalts [8], as well as synthetic binders [9,10] or de-colored bitumens [11]. Among these, clear resins can be produced through synthetic processes to obtain yellowish/transparent binders, with adhesiveness and mechanical properties comparable to those of conventional asphalts [12,13]. Their recent diffusion in the paving

industry is noted because of the growing consideration directed toward more sustainable pavements (aesthetic concerns, landscape preservation, low thermal impact, etc.) [14,15].

Nowadays, the analysis of synthetic binders, referring to their mechanical characterization, still also represents a challenge for researchers because of their complex behavior. With respect to conventional bitumens, the common rheological approaches and testing protocols often fail in properly describing the rheology of the synthetic binders [16]. The above-mentioned rheological complexity, determined by a complex chemical structure [17], can be variably linked to different factors such as non-conventional visco-elastic behaviors [18], marked non-linear responses at in-field stress–strain levels [5], possible relaxations, glassy or transition phenomena (typical of non-Newtonian fluids) [19], variable susceptibility to aging [20] and steric hardening [21] (often resulting in misleading stiffness detections). This complexity can be easily detected performing standard rheological tests. For instance, Black diagrams (displaying material stiffness vs. phase angle at different times and temperatures) provide initial proof of such aspects (i.e., dominant behavior in terms of elasticity, viscosity, ductility, brittleness, etc.). Few publications about synthetic binders within the sector literature can be found. As an example, based on a variety of stress, time and temperature tests, a clear synthetic binder was found to behave discontinuously due to a phase transition, presenting poor stiffness at high temperatures, as well as great hardness at low ones, with probable implications related to thermal cracking [13]. For an analogy, three clear synthetic binders were found to show thermorheologically complex behaviors, alternatively exhibiting asymptotical responses to the glassy limit or pure viscous flow state, or discontinuities in the phase angle domain; this was ascribed to the melting of wax-like constituent materials or the presence of different solid-like components which generate a rubbery-like plateau [22]. A rheological complexity was also detected for polyethyl-acrylate, polymethyl-acrylate and polybutyl-acrylate binders that, in certain cases, demonstrated considerably polymer-like behavior, such as variable consistency and a greater viscosity with respect to conventional binders [19]. In turn, a clear synthetic resin studied with conventional rheological protocols behaved as a soft material susceptible to permanent deformation, but also able to postpone fatigue cracking (variable rheological behavior as a function of the in-service temperature) [23].

2. Objective and Research Approach

Given this background, the main objective of the research surrounds the attempt to define specific advancements in the rheological protocols used for binder characterization, in particular when unconventional materials are tested. The study presents an advanced rheological approach for describing a synthetic binder for paving (bicomponent resin binder) suitable for the production of sustainable and thermally optimized road pavements able to mitigate the phenomenon of the urban heat island (due to their thermal properties like albedo, Solar Reflectance Index, emissivity, conductivity, etc.). Such advances could bridge the existing knowledge gap because the traditional tests and elaborations for conventional bituminous binders are ineffective. In fact, specific studies addressing the modeling of the complex rheological behavior of synthetic binders for pavement purposes cannot be found in the literature. To this aim, the research analysis was organized to subsequently investigate the following aspects:

1. plain rheological behavior of binders (time–temperature superposition concerns for bituminous and synthetic binders);
2. preliminary conditions for complex rheological behavior (analysis of steric hardening, time–temperature dependency and the linear visco-elastic (LVE) region, localizing the assumptions of linearity/thermorheological simplicity);
3. complex rheological behavior of binders (to furnish a comprehensive report concerning their expected mechanical responses).

To accomplish these objectives, several rheological tests developed through the Dynamic Shear Rheometer (DSR) were executed to establish a prompt laboratory protocol

able to adequately summarize the responses of the selected synthetic innovative material subject of this study.

3. Materials

The synthetic binder (hereafter coded SB) selected for the experimentation was a commercial product used in the manufacturing of the wearing course of clear roads. In fact, thanks to its chromatic characteristics, it could also be used to magnify the chromatic properties of the lithic matrix of the paving mixtures to obtain clear pavement layers (in the semi-liquid state, the binder has a yellow/amber tint). This proprietary material was generated by a synthetic fluid catalyst, within which a solid granular phase was dispersed. At ambient temperature, it resulted in a homogeneous thermoplastic bicomponent binder. The viscosity at the conventional temperatures used for the mix manufacture (160–170 °C) guaranteed suitable film thicknesses and bonding behavior within the produced mixture. Also, a reference plain 70/100 bituminous binder (hereafter indicated with BB) provided by an asphalt plant in Northern Italy was selected for the experimentation with comparative purposes. Being a non-polymer-modified binder, BB was proposed to present the simple rheological behavior of a conventional paving bitumen. A preliminary empirical characterization carried out in the laboratory on both binders, whose results are presented in Table 1, already indicated noticeable differences in their basic physical properties (i.e., greater high-service temperature consistency and lower mid-service temperature ductility for SB). To obtain the specimens for DSR testing, both binders were oven-heated at 165 °C for 1 h 30 min to reach adequate viscosity for pouring. Then, they were poured in ad-hoc silicon molds having diameters of 8 or 25 mm and heights exceeding 2 or 1 mm, respectively. Molds were cooled and stored at ambient temperature for 1 day before testing. Since the whole experimental protocol takes a significant amount of time, sample pro-duction was progressively repeated with identical batches to avoid discrepancy in binders' ages at different experimental times. Figure 1 illustrates an example of the manufactured specimens.

Table 1. Physical properties of the tested binders.

Property	SB	BB	Standard
Penetration at 25 °C	72 dmm	77 dmm	EN 1426
Softening point	59 °C	43 °C	EN 1427
Ductility at 25 °C	230 mm	>1000 mm	CNR 44
Fraass breaking point	−7.5 °C	−8.2 °C	EN 12593
Penetration at 25 °C (after RTFO)	55 dmm	52 dmm	EN 12607-1
Softening point (after RTFO)	64 °C	50 °C	EN 12607-1

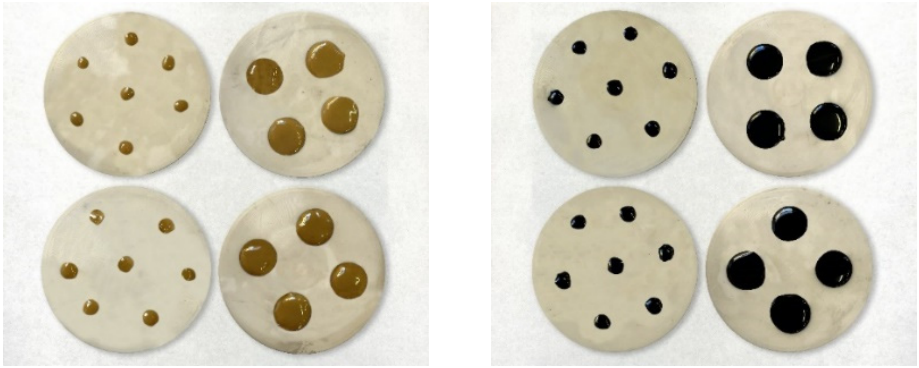

(**a**) (**b**)

Figure 1. Samples for DSR testing: SB (**a**) and BB (**b**).

4. Testing Methods

As anticipated, a comprehensive laboratory DSR survey was executed. Two testing geometries (PP08 or PP25 plate–plate measuring systems) were used for low-intermediate- and high-temperature testing, respectively. More details about DSR testing conditions can be found within the EN 14770 (2012) standard. It was worth specifying that each experimental result was checked in terms of output torque (M) to ensure reliable calculations of the output physical quantities (DSR torque range limit: 0.5 nNm–200 mNm).

4.1. Plain Rheological Behavior of Binders

Frequency Sweep (FS) oscillatory tests were carried out to determine the overall visco-elastic behaviors of the selected binders, imposing a constant low-strain amplitude equal to 0.5% within the linear domain (LVE region commonly achieved at strains lower than 1.0% [24]). The angular frequency ω was in the range of 0.1–100 rad/s between a T of 10 and 60 °C using PP08 and between 20 and 80 °C (T step of 5 °C) using PP25. Three test replicates were executed for each specimen. Initially, samples were thermally stabilized at each testing T for 20 min, which has been well-established by several DSR testing protocols [25]. The collected results were used to produce the Black diagrams, also assessing the possible construction of $|G^*|$ and δ Master Curves (MCs) based on a well-known rheological approach extensively described elsewhere [26,27]. In this sense, Figure 2 shows typical Black curves for different asphalt materials [28].

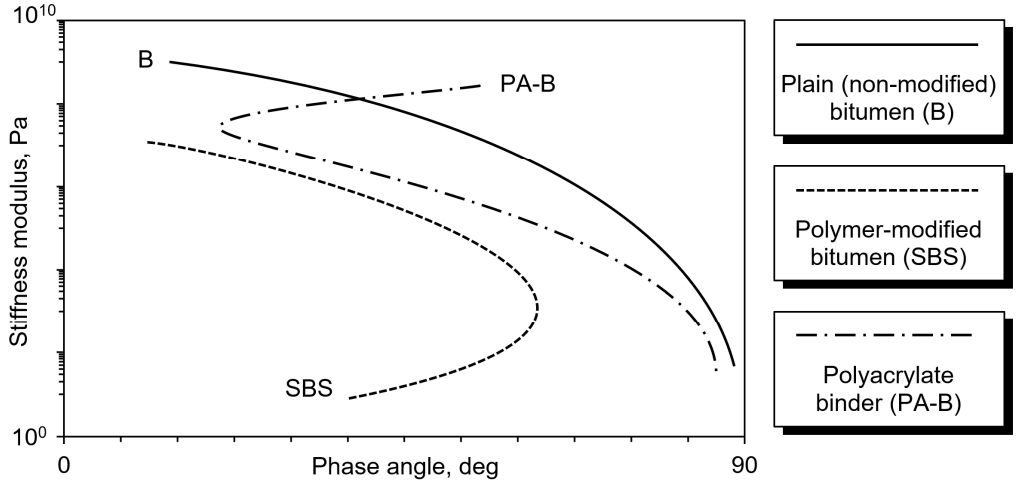

Figure 2. Typical Black curves for different asphalt materials.

4.2. Preliminary Conditions for the Complex Rheological Behavior

Specific trials were planned to investigate various testing aspects influencing the experimental readings of stiffness and phase angle.

Firstly, possible steric hardening at ambient temperature was evaluated. It consists of a reversible physical stiffening (leading to $|G^*|$ overestimations) [29] due to thermal expansion and alteration of the sample thickness [21]. In this sense, tests on SB were drawn to establish a suitable conditioning time (t_{cond}) for the prevention of steric hardening (normal force N was continuously controlled during tests to maintain the sample geometry).

Then, an analysis was executed to check the time–temperature-dependent behavior of SB. To this aim, DSR tests were carried at various setting combinations with two sampling protocols (i.e., FS-A or FS-B). With FS-A (as performed in the previous research stage), each data point was recorded once before sweeping. With FS-B, each data point was repeatedly collected at the same setting before sweeping (10 pts for each setting).

Finally, the proper linear visco-elastic region of SB was investigated. BB was also studied for comparison. Being strictly dependent on the consistency and the test setting, the linear visco-elastic (LVE) limit is often overlooked, or sketchily investigated with few explorative trials conducted to avoid time-consuming protocols. In this study, several

Amplitude Sweep (AS) oscillatory tests were executed to calculate the LVE strain limits under representative couples of T and ω (three test replicates). Each AS was developed at a unique T and ω, applying a strain sweeping from 0.01 to 100% (log ramp with 10 pt increments). Each binder specimen was conditioned before the test according to previous findings about t_{cond}. LVE strain limits were calculated using the common approach of a 5% reduction of the initial complex stiffness modulus [18].

All the selected parameters for the described tests are summarized in Table 2.

Table 2. DSR settings for tests about preliminary conditions.

Test Series 1—Analysis of t_{cond}						
T	γ	ω		**PP**	***N***	***t***
10 °C	0.5%	0.1, 1, 10 or 100 rad/s (constant)		PP08	0 N (constant)	60 min
40 °C	0.5%	0.1, 1, 10 or 100 rad/s (constant)		PP08	0 N (constant)	60 min
70 °C	0.5%	0.1, 1, 10 or 100 rad/s (constant)		PP25	0 N (constant)	60 min
Test Series 2—Analysis of *t*-*T* Dependency						
T	γ	ω	t_{cond}	**PP**	***N***	**Protocol**
10 °C	0.5%	0.1 to 100 rad/s	*	PP08	0 N (constant)	FS-A
40 °C	0.5%	0.1 to 100 rad/s	*	PP08	0 N (constant)	FS-A
70 °C	0.5%	0.1 to 100 rad/s	*	PP25	0 N (constant)	FS-A
10 °C	0.5%	0.1 to 100 rad/s	*	PP08	0 N (constant)	FS-B
40 °C	0.5%	0.1 to 100 rad/s	*	PP08	0 N (constant)	FS-B
70 °C	0.5%	0.1 to 100 rad/s	*	PP25	0 N (constant)	FS-B
Test Series 3—Analysis of LVE Limit						
T	γ	ω	t_{cond}	**PP**		***N***
10 °C	0.01 to 100%	0.1, 1, 10 or 100 rad/s (const.)	*	PP08		0 N (const.)
25 °C	0.01 to 100%	0.1, 1, 10 or 100 rad/s (const.)	*	PP08 **		0 N (const.)
40 °C	0.01 to 100%	0.1, 1, 10 or 100 rad/s (const.)	*	PP25 **		0 N (const.)
55 °C	0.01 to 100%	0.1, 1, 10 or 100 rad/s (const.)	*	PP25		0 N (const.)
70 °C	0.01 to 100%	0.1, 1, 10 or 100 rad/s (const.)	*	PP25		0 N (const.)

* To be established based on Test series 1 outcomes. ** PP08 or PP25 (variable depending on the selected binder).

4.3. Complex Rheological Behavior of Binders

In the core phase, common DSR test protocols were adjusted. The steady-state transient approach (within the linear low-strain domain) was passed over considering the larger deformations experienced in in-service real-scale road pavements subject to rutting or cracking phenomena. Thus, a set of advanced tests was planned to also allow for work within the non-linear visco-elastic range (higher strain amplitudes), giving a complete report of binder mechanical performance. With respect to rheology in large stress–strain fields, the non-linearity should be considered to evaluate various superimposed effects regarding physical, kinetic and phase contributions [30]. To this aim, tests at constant strain rates ($\dot{\gamma}$) were executed on SB at fixed temperatures (from 10 to 80 °C, with 5 °C variation step) using PP08 and PP25 geometries (2 replicates for each test configuration). The application of constant shear rates implied the simultaneous sweeping of both the angular frequency and the applied strain (strain amplitude inversely proportional to the oscillation angular frequency). Since the γ was sweeping, it was not needed to care about the LVE limits (the non-linear visco-elastic region could be entered). BB was no longer tested since the conventional testing protocol is commonly assumed to reliably describe its rheological behavior.

Table 3 reports all the experimental details. Data elaborations were based on the Strain-Rate Frequency Superposition (SRFS) principle [31], considering the time scale dependency on the applied strain rate, similarly to the common TTS approach for temperature.

Table 3. Details of DSR tests executed at constant strain rates.

T	$\dot{\gamma}$	γ	ω	t_{cond}	PP	N
10 to 80 °C (5 °C step)	0.001 s^{-1} (const.)	0.01 to 100%	10 to 0.1 rad/s	*	**	0 N (const.)
	0.005 s^{-1} (const.)	0.1 to 10%	5 to 0.05 rad/s	*	**	0 N (const.)
	0.01 s^{-1} (const.)	0.01 to 10%	100 to 0.1 rad/s	*	**	0 N (const.)
	0.05 s^{-1} (const.)	0.1 to 10%	50 to 0.5 rad/s	*	**	0 N (const.)
	0.1 s^{-1} (const.)	0.1 to 100%	100 to 0.1 rad/s	*	**	0 N (const.)
	0.5 s^{-1} (const.)	1 to 100%	50 to 0.5 rad/s	*	**	0 N (const.)
	1 s^{-1} (const.)	1 to 100%	100 to 1 rad/s	*	**	0 N (const.)
	5 s^{-1} (const.)	1 to 100%	50 to 5 rad/s	*	**	0 N (const.)

* To be established based on Test series 1 outcomes. ** PP08 or PP25 (variable depending on the selected binder).

Figure 3 summarizes all the research stages described above.

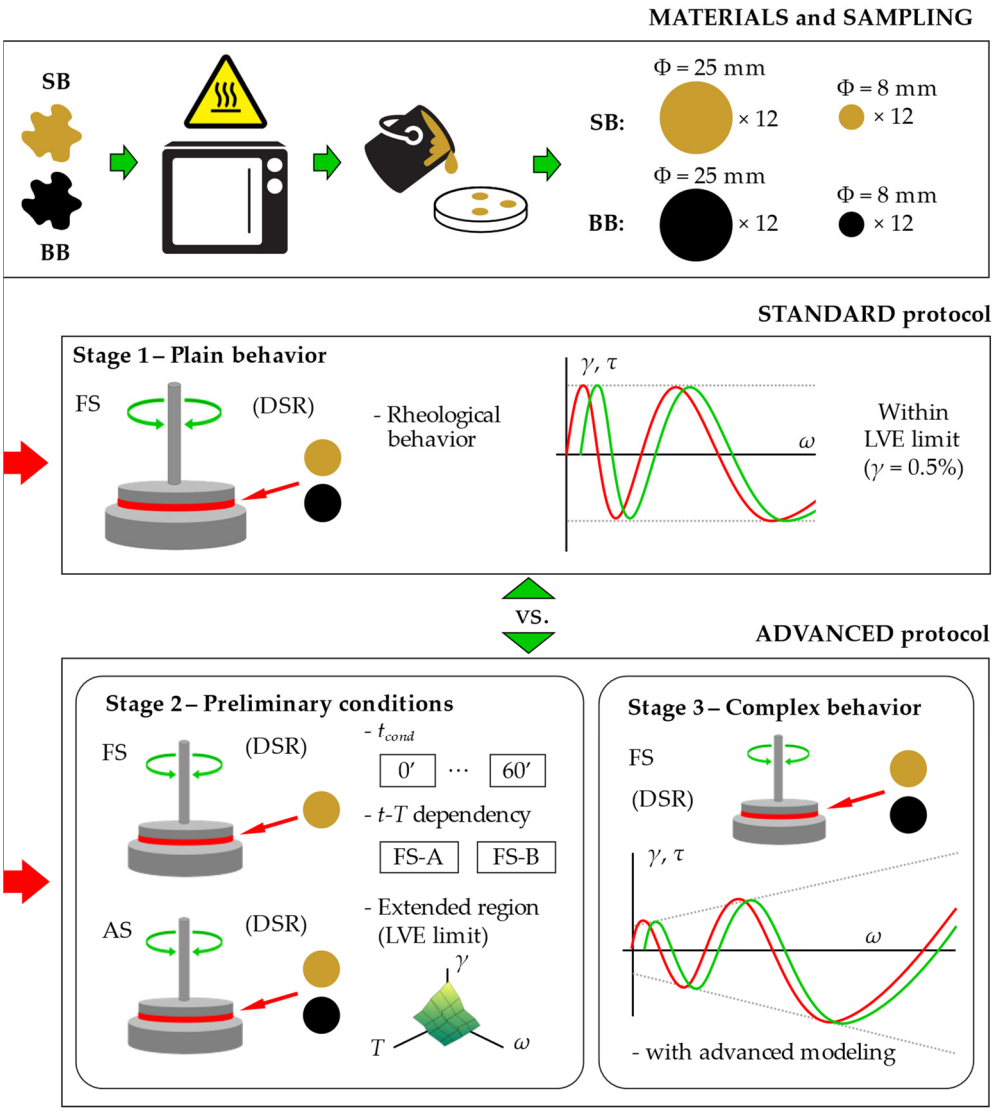

Figure 3. Summary of the experimental plan stages.

5. Results, Analysis and Discussions

5.1. Plain Rheological Behavior of Binders

The plain rheological response of the tested binders, assessed within their linear domains, is represented in the black space in Figure 4 as an average of the three replicates. As expected, BB was characterized by a smooth, uniquely aligned curve that certified

the material's thermorheological simplicity, whereas SB assumed a complex, bell-shaped behavior (already discussed elsewhere [23]). At the present stage, the disruption of the experimental curve for SB could be attributed to the rheological complexity of the synthetic binder only because:

1. the loss of linearity should be averted thanks to the low strain constantly applied during the DSR test (0.5%);
2. the torque limits related to equipment compliance were never exceeded during the tests;
3. a good repeatability between the three test replicates was obtained for SB.

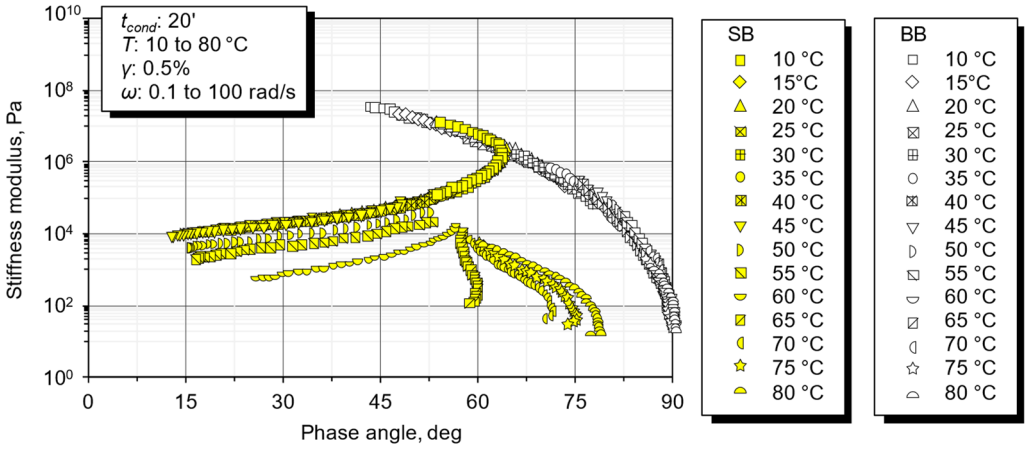

Figure 4. Black diagram of binders SB and BB.

Thus, the TTS principle could be questionable in this case, and the MCs of BB and SB (Figure 5) confirmed this finding (SB could not be modeled with conventional elaborations). Within Figure 5, MCs are arbitrary plotted at the reference temperature T_0 of 40 °C.

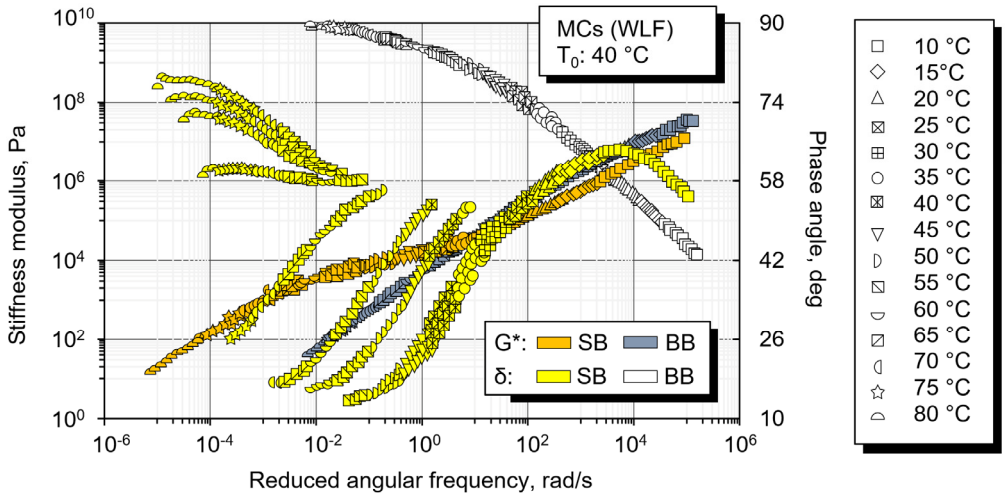

Figure 5. Conventional MCs of binder SB and BB.

5.2. Preliminary Conditions for the Complex Rheological Behavior

With respect to steric hardening, the effect of time is depicted in Figure 6, where $|G^*| \cdot sin\delta$ parameter is plotted as a function of time at various combinations of T and ω (average of three test replicates). The evolutive response during the time indicated that each sample owned an initial stabilization phase (credibly ascribed to the time needed to reach thermal equilibrium within the sample). Neither the angular frequency (0.1, 1, 10 or 100 rad/s), nor the temperature (10, 40 or 70 °C) seemed to be an influence with respect to this initial time. The bigger red markers are depicted in correspondence with the stabilization threshold of the $|G^*| \cdot sin\delta$ values, which were fixed when the data variation became lower

than 0.5%. Over a long period, a constant response was detected up to 60 min. All facts suggested that to avoid steric hardening, a t_{cond} of 15 min was appropriate.

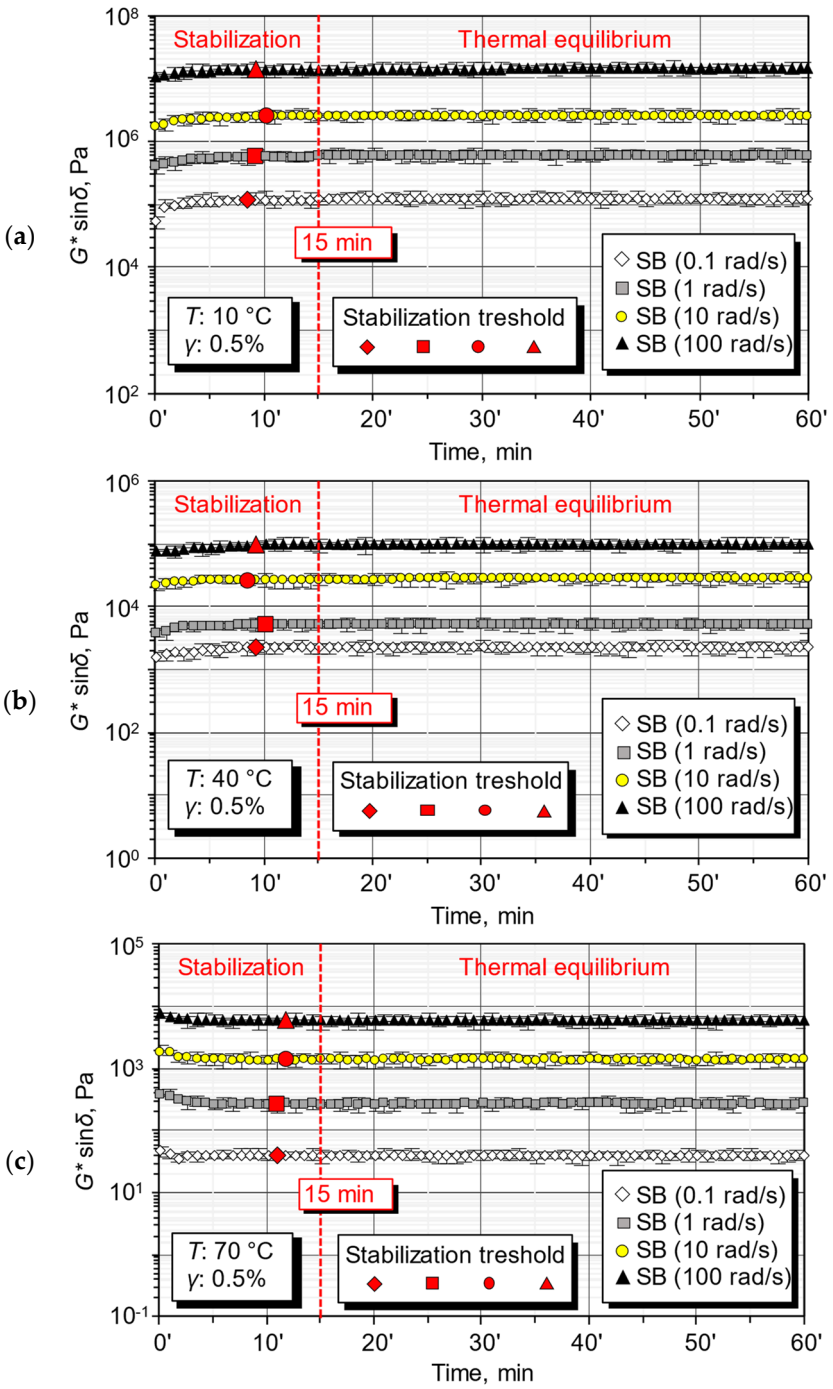

Figure 6. Evolution in the time of $|G^*| \cdot sin\delta$ for tests at 10 °C (**a**), 40 °C (**b**) and 70 °C (**c**).

Then, FS-A and FS-B protocols were compared (average of three data series) to assess the time–temperature dependency.

Based on AASHTO T315-20 (2020) and ASTM C670 (2015) standards, a satisfactory single-operator testing repeatability was obtained for the unconventional FS-B protocol (with a 95% confidence level, $|G^*|$ and δ variabilities did not exceed the standard deviation prescribed limits). For the sake of brevity, Table 4 shows the precision results related to 10 °C tests only. A comparison between the outputs of FS-A and FS-B is given in Figure 7: here, average storage (G') and loss (G'') moduli are plotted against the ω for some indicative

T (lines represent the FS-A trends and markers indicate FS-B data). Based on trends and error bars, it was stated that the two testing protocols led to analogous results within the whole ω range. Therefore, a single-point recording protocol (conventional FS-A) was considered enough to describe the response of the material, saving the huge testing time implied by the more complex FS-B set up.

Table 4. Precision of $|G^*|$ and δ recorded through FS-B protocol (example: T = 10 °C).

ω	$\Delta\|G^*\|$, Pa	$\|G^*\|_{limit}$, Pa	$\Delta\delta$, deg	δ_{limit}, deg
0.1 rad/s	2.98×10^3	4.34×10^3	0.233	0.285
0.2 rad/s	1.45×10^3	1.86×10^3	0.05	0.069
0.3 rad/s	1.51×10^3	1.85×10^3	0.072	0.105
0.4 rad/s	2.05×10^3	2.52×10^3	0.057	0.082
0.5 rad/s	1.49×10^3	1.78×10^3	0.048	0.073
0.6 rad/s	1.83×10^3	2.22×10^3	0.024	0.035
0.7 rad/s	1.96×10^3	2.32×10^3	0.039	0.05
0.8 rad/s	1.07×10^3	1.29×10^3	0.029	0.039
0.9 rad/s	1.12×10^3	1.51×10^3	0.017	0.025
1 rad/s	1.16×10^3	1.32×10^3	0.015	0.022
2 rad/s	1.30×10^3	1.99×10^3	0.02	0.024
3 rad/s	1.24×10^3	2.09×10^3	0.011	0.013
4 rad/s	2.43×10^3	3.60×10^3	0.005	0.006
5 rad/s	2.15×10^3	3.03×10^3	0.006	0.008
6 rad/s	1.26×10^3	1.89×10^3	0.003	0.004
7 rad/s	3.34×10^3	4.24×10^3	0.005	0.005
8 rad/s	1.46×10^3	2.40×10^3	0.003	0.004
9 rad/s	2.15×10^3	3.64×10^3	0.004	0.006
10 rad/s	2.98×10^3	4.31×10^3	0.002	0.004
20 rad/s	3.93×10^3	5.79×10^3	0.004	0.005
30 rad/s	4.12×10^3	6.02×10^3	0.004	0.005
40 rad/s	7.79×10^3	9.68×10^3	0.006	0.007
50 rad/s	5.49×10^3	7.17×10^3	0.005	0.006
60 rad/s	7.13×10^3	1.08×10^4	0.005	0.007
70 rad/s	5.46×10^3	6.95×10^3	0.004	0.005
80 rad/s	1.32×10^4	1.79×10^4	0.009	0.012
90 rad/s	1.09×10^4	1.74×10^4	0.008	0.012
100 rad/s	1.73×10^4	2.12×10^4	0.012	0.014

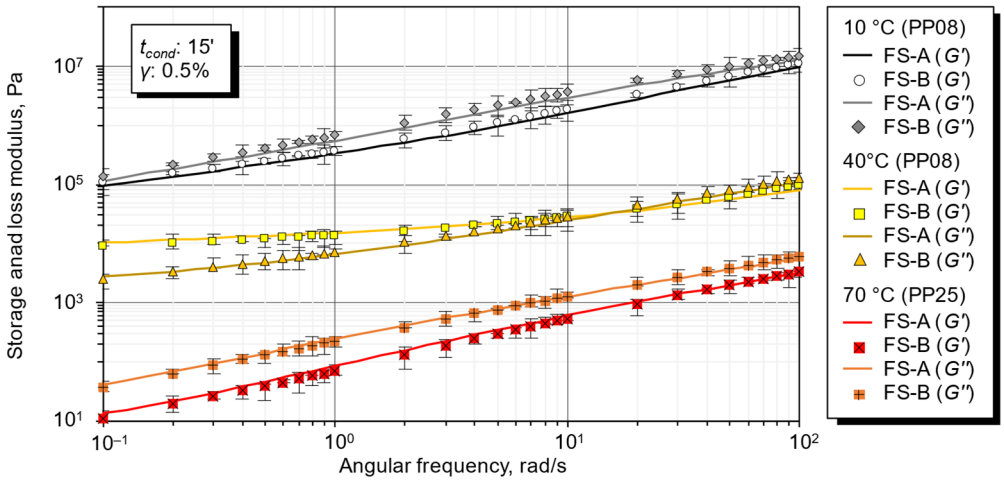

Figure 7. Comparison of FS-A and FS-B protocols.

Finally, the LVE domains of SB and BB are depicted in Figure 8 (replicate's average of LVE limits vs. T and ω). The influence of the T and ω on the different visco-elastic

responses could easily be observed based on the isochronal and isothermal plots reported in Figures 9 and 10, respectively. As commonly achieved for bitumens, the temperature effect was opposite to that of the angular frequency (as expected, the increase of ω was more and more of an influence when increasing the test temperature). In contrast, for SB, the ω increase produced a quasi-linear increase of the LVE transitions regardless of T. Up to the intermediate temperatures, the LVE limits for SB were generally higher than those of BB. Starting from about 40 °C, SB and BB responses started to completely differ, above all with respect to the lower analyzed frequencies. In terms of LVE limit, at 70 °C, SB experienced a tendency inversion with respect to 60 °C at any fixed ω (this was likely due to the complex/discontinuous rheological behavior of SB). The calculated LVE trends were kept into account for further linear/non-linear complex analyses.

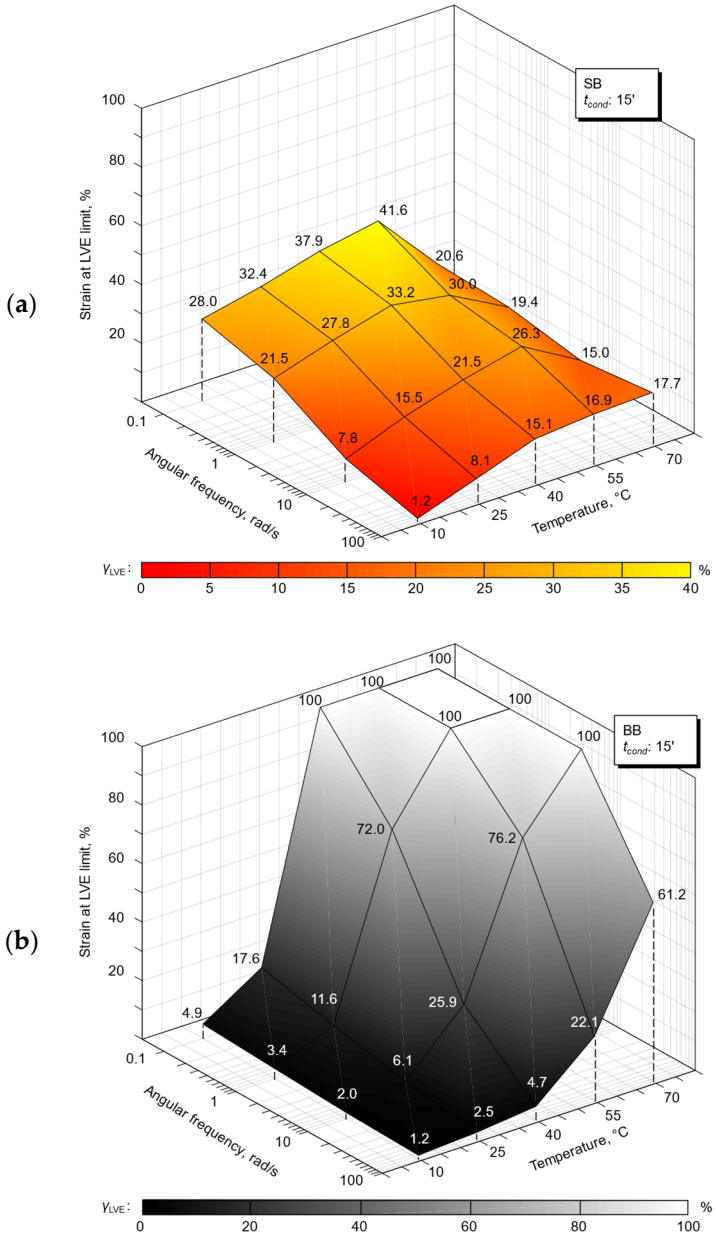

Figure 8. LVE limit domain for SB (**a**) and BB (**b**).

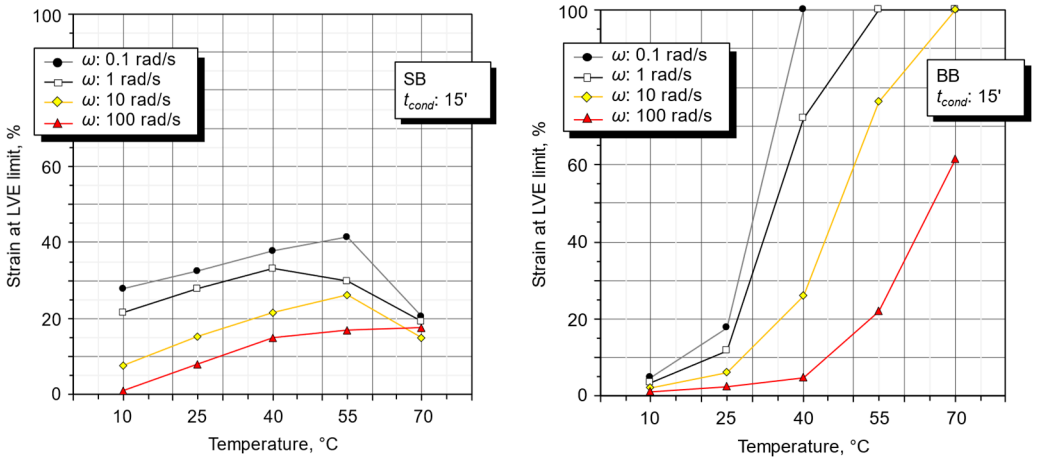

Figure 9. Isochronal plots of LVE limits for SB (**a**) and BB (**b**).

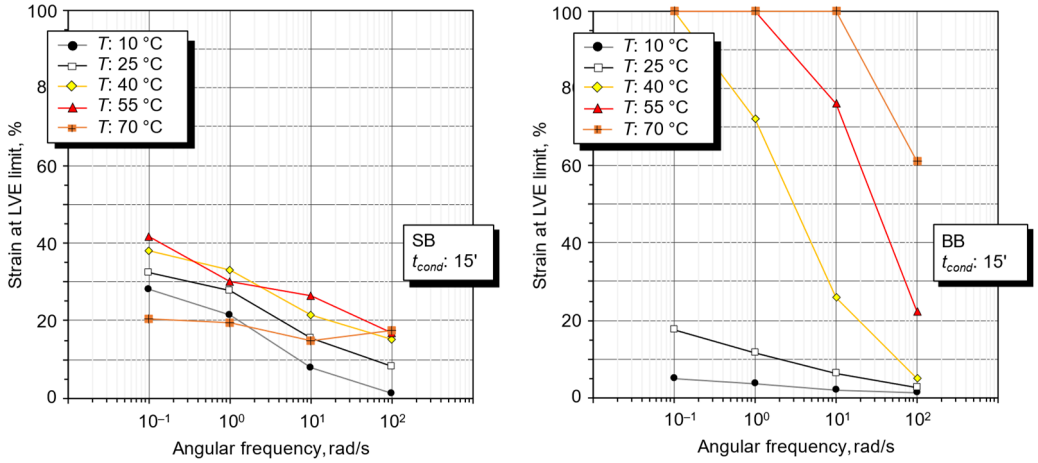

Figure 10. Isothermal plots of LVE limits for SB (**a**) and BB (**b**).

5.3. Complex Rheological Behavior of Binders

Dealing with the synthetic binder SB, Figure 11 relates the experimental parameters chosen for each constant-rate test with the LVE limits interpolated from the previous analysis (analysis field extended up to the DSR torque limits). Here, the marker shape refers to tested temperatures for both linear (yellow markers) and non-linear (red markers) experimental data.

Experimental results obtained for SB are plotted in the Black Diagram of Figure 12 where, at each T, the $|G^*|$–δ couples recorded within the non-linear fields are highlighted in red color. With respect to the disrupted Black curve obtained for SB though the conventional rheological FS tests (see Figure 4), a sort of partially aligned trend (quasi-continuous binder behavior) seemed to be visible.

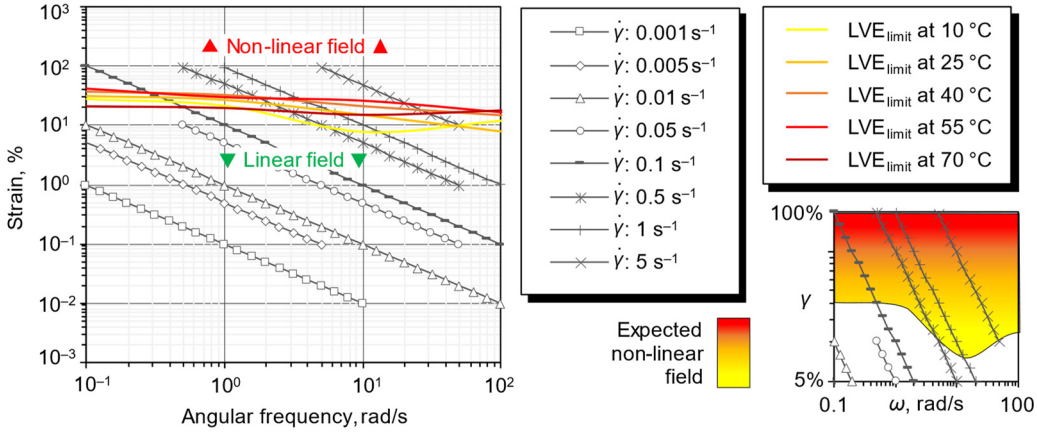

Figure 11. Comparison between the constant-rate test and the LVE limits for SB binder.

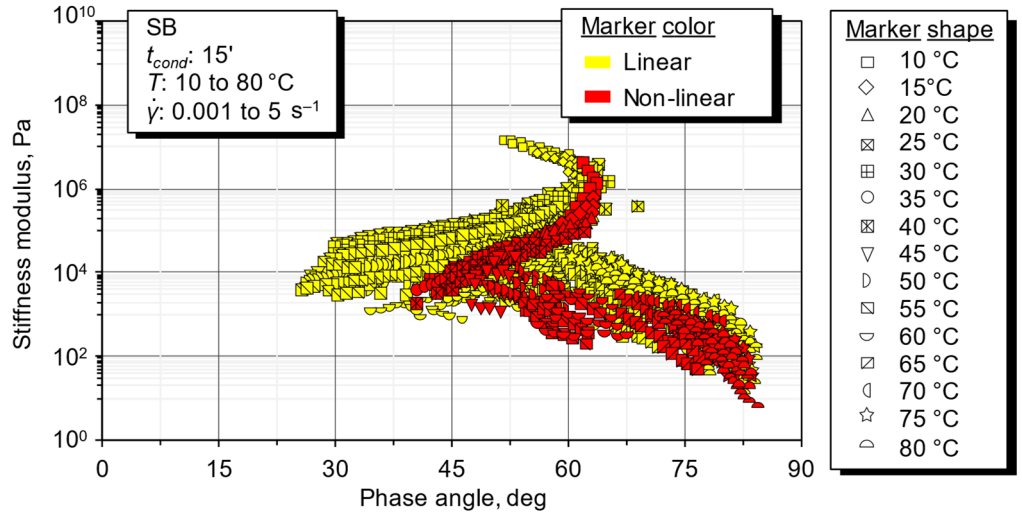

Figure 12. Black plot of SB binder showing output of constant-rate tests entering non-linear field.

Based on this consideration, further elaborations were proposed to deal with the non-linear recorded data to be more representative of the large stress–strain fields, typically linked to pavement rutting or cracking phenomena. Starting from the strain rate definition in Equation (1), the physical quantities of stiffness and phase angle can be related according to Equations (2)–(4) (the strong dependency of the visco-elastic response on the strain rate magnitude suggested the following of such a novel approach).

$$\dot{\gamma}_0 = \gamma \cdot \omega \tag{1}$$

$$\dot{\gamma} = \gamma_0(t) \cdot \sin(\omega t) \tag{2}$$

$$\tau(t) = \tau_0(t) \cdot \sin(\omega t + \delta) = \tau_0(t) \cdot \cos\delta \cdot \sin\omega t + \tau_0(t) \cdot \sin\delta \cdot \cos\omega t \tag{3}$$

$$G* = \frac{\tau_0(t)}{\gamma_0(t)} \cos\delta + \mathrm{i} \cdot \frac{\tau_0(t)}{\gamma_0(t)} \sin\delta \tag{4}$$

The construction of a singular MC of the non-linear SB behavior was attempted. This was done by rescaling the $|G^*|$–ω and δ–ω plots as a function of both $\dot{\gamma}$ and T, according to Equations (5) and (6).

$$G*_{\text{scaled}}(\omega) = b_{nl}(T, \dot{\gamma}) \cdot G*(\omega / a_{nl}(T, \dot{\gamma})) \tag{5}$$

$$\delta_{\text{scaled}}(\omega) = b_{nl}(T, \dot{\gamma}) \cdot \delta(\omega / a_{nl}(T, \dot{\gamma})) \tag{6}$$

Here, $a_{nl}(T,\dot{\gamma})$ and $b_{nl}(T,\dot{\gamma})$ indicate the shift factors in the horizontal and vertical scales, respectively, that are dependent on both the temperature and the strain rate amplitude. The obtained master curves for the non-linear complex stiffness modulus and phase angle are presented in Figures 13 and 14 (the reference temperature T_0 was arbitrarily set as equal to the intermediate T of 40 °C. The reference strain rate $\dot{\gamma}_0$ was selected at 0.1 s^{-1} since the corresponding behavior was similar to that associated with the conventional sweep at a constant strain amplitude).

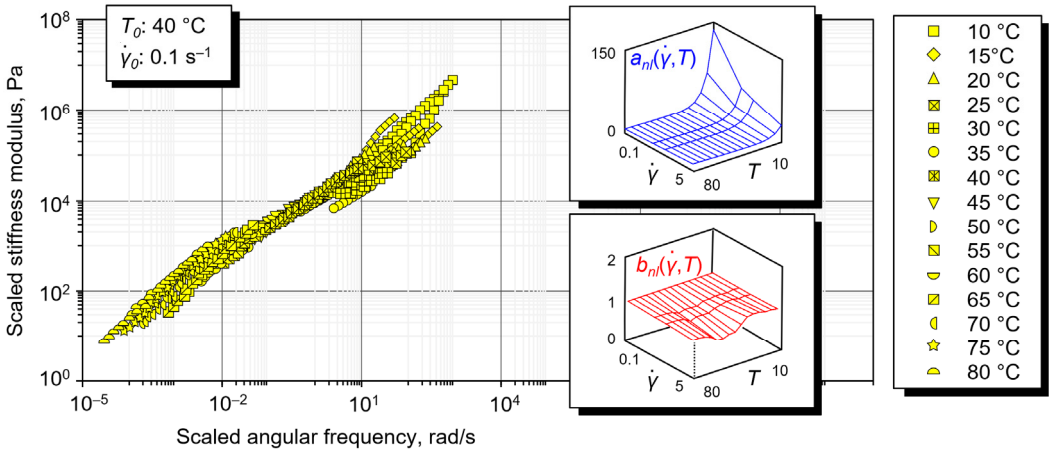

Figure 13. Non-linear MC of binder SB showing complex stiffness modulus vs. angular frequency.

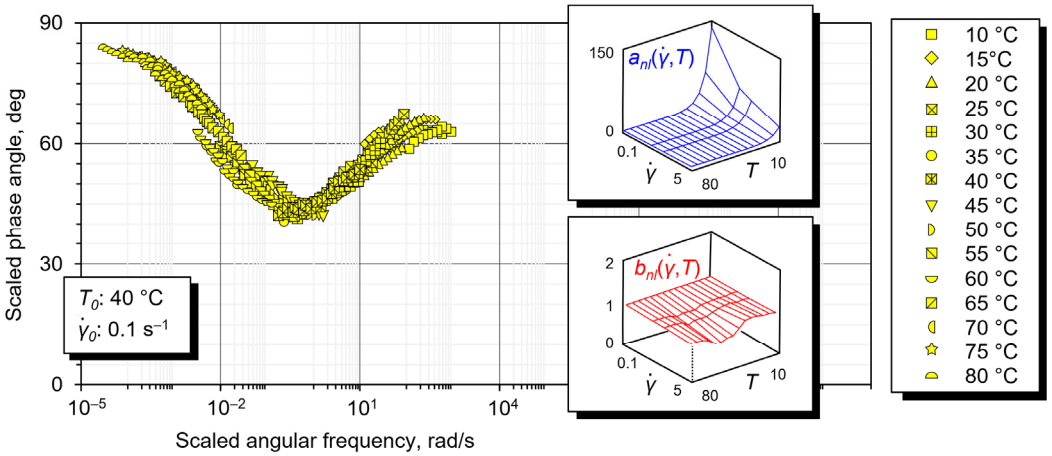

Figure 14. Non-linear MC of binder SB showing phase angle vs. angular frequency.

An acceptable scattering of data producing quasi-smoothed curves was obtained using the same shifts for G^* and δ. Data fitting was performed, resulting in continuous trends which were verified to match the relationships presented in Equations (7) and (8), with coefficients of determination R^2 of 0.9458 and 0.9026 for $a_{nl}(T,\dot{\gamma})$ and $b_{nl}(T,\dot{\gamma})$, respectively.

$$a_{nl}(T,\ \dot{\gamma}) = 10^{K(T-T_0)} \cdot C_1(T) \cdot \dot{\gamma}^{C_2(T)} \tag{7}$$

$$b_{nl}(T,\ \dot{\gamma}) = C_3(T) \cdot \dot{\gamma}^{C_4(T)} \tag{8}$$

The inset plots within Figures 13 and 14 depict the fitting laws for the scaling factors (the figures report the same insets because the same a and b factors were used for both the G^* and δ master curves). $C_1(T)$, $C_2(T)$, $C_3(T)$ and $C_4(T)$ are fitting parameters that were dependent on the analyzed temperature; K represents a $\dot{\gamma}$-independent fitting parameter. Based on the fitting equations, the following conclusions can be drawn:

- for $a_{nl}(T,\dot{\gamma})$ (horizontal scale factor), the temperature T had a linear effect on shifting, similar to that widely experienced in conventional T-scaling through the relation of the $log(a_T) = C \cdot (T - T_0)$ [32], whereas the strain rate $\dot{\gamma}$ contribution could be modeled through a power law relation;
- for $b_{nl}(T,\dot{\gamma})$ (vertical scale factor), the temperature was not an influence; thus, a power-type fitting law related to the strain rate was only enough to model the vertical scaling.

Then, it was further verified that the T-dependent fitting parameters $C_1(T)$, $C_2(T)$, $C_3(T)$ and $C_4(T)$ could be linked to the temperature through reliable linear interpolations of the type $C_i = h_i \cdot T + j_i$ in Equations (9)–(12), where h_i and j_i are the linear fit coefficients (coefficient of determination R^2 always greater than 0.89). For the sake of completeness, all the fitting results are indicated in the following table (Table 5).

$$C_1(T) = h_1 \cdot T + j_1 \quad (9)$$

$$C_2(T) = h_2 \cdot T + j_2 \quad (10)$$

$$C_3(T) = h_3 \cdot T + j_3 \quad (11)$$

$$C_4(T) = h_4 \cdot T + j_4 \quad (12)$$

Table 5. Fitting coefficient for horizontal and vertical shift factors.

Fitting Coefficient *K* −0.0721								
Coefficients for $C_1(T)$, $C_2(T)$, $C_3(T)$ and $C_4(T)$								
***T*, °C**	**h_1 ($\times 10^{-3}$)**	**j_1 ($\times 10^{-1}$)**	**h_2 ($\times 10^{-3}$)**	**j_2 ($\times 10^{-1}$)**	**h_3 ($\times 10^{-3}$)**	**j_3 ($\times 10^{-1}$)**	**h_4 ($\times 10^{-3}$)**	**j_4 ($\times 10^{-3}$)**
10–35	1.949	3.010	3.601	−5.260	−0.438	10.06	0.602	0.249
40–60	−2.444	4.529	−2.840	−2.852	−5.096	11.40	2.920	90.80
65–80	16.601	−6.372	11.16	−10.43	4.468	6.372	1.360	121.1

In the final step of the study, the physical indications given by the new, non-linear approach were evaluated in comparison with that evinced from the first research step (Figure 5 vs. Figures 13 and 14).

At a first glance, non-linear MCs are able to emphasize the structural relaxation phenomena suffered by SB at a high temperature and low consistency [30]. In general, SB was softer than BB for the greater part of the ω domain and this seemed to accord with existing empirical and rheological findings of previous stages.

A closer inspection of δ within the non-linear plot indicated a SB response deeply different from BB (information not detected with the conventional approach). For comparison, SB was tendentially more elastic with respect to BB (lower δ values in the whole ω range). But based on Figure 14, above about 0.5–2 rad/s, SB had a local inverse behavior with respect to BB (δ increasing with ω). At the lowest T, a further curvature is slightly visible in the δ data (specific low-temperature tests could clarify if further tendency inversions or a plateau stabilization could be present). In addition, the non-monotonous shape of the δ non-linear curve allowed for the location of two distinct SB crossover frequencies (at which $\delta = 45°$) at about 0.1 and 2 rad/s, within which the elasticity dominates.

Such a finding, that is quite uncommon for conventional plain road bitumens, would not be visible without analyzing the non-linear MC (the data dispersion of the conventional Black plot or linear MCs would have hidden this information).

6. Conclusions and Prospects for Further Studies

The present research dealt with the rheological characterization of clear synthetic resins used in the paving industry to obtain sustainable thermally optimized pavements. Advances in the rheological testing and elaboration protocols of such materials were

proposed based on an extended DSR laboratory investigation. The experimental data and proposed modeling suggested the following considerations:

- the synthetic binder presented an initial relaxation phenomenon that suggested the adoption of a conditioning time equal to 15 min; no specific steric hardening was experienced with the long testing period;
- the visco-elastic behavior of the synthetic binder was very different compared to a reference plain road bitumen;
- it was possible to implement an advanced DSR protocol imposing constant strain rates in oscillatory mode in order to enter the non-linear visco-elastic region to collect info about the large stress–strain fields, typically linked to pavement rutting or cracking phenomena;
- feasible master curves of the non-linear rheological data were constructed; this was made through horizontal and vertical scaling factors (function of the temperature and the strain rate) based on linear and power law equations;
- such master curves resulted in additional advice about the rheological response of the synthetic resin with complex behavior, above all with respect to phase angle.

All things considered, it could be concluded that the implementation of innovative constant-strain rate oscillatory DSR tests, and the specific evaluation of non-linear data, implying the large strains usually linked to rutting or cracking, could be a valid tool to collect new rheological outcomes when dealing with rheologically-complex materials, such as synthetic resins. In this sense, the proposed protocol could contribute to the promotion of the use of such products in the paving industry by highlighting its overall sustainability related to different environmental and economic impacts (in this regard, it is reported that, for example, the tested binder would imply 20% higher costs with respect to conventional bituminous binders).

Some research efforts are being planned to continue the validation of the proposed method. This will enlarge the experimental domain (e.g., towards the low in-service temperature) and extend the approach to various non-conventional binders with similar complexity. Modeling could be also aimed at defining physically significant fittings, as commonly admitted for traditional bituminous binders. Nonetheless, an extended mixture-scale testing is planned to validate the mechanical indications given by the studied rheology.

Author Contributions: Conceptualization, A.B.; methodology, A.B. and E.P.; software, A.B. and E.P.; validation A.B. and G.G.; formal analysis, M.P. and G.G.; investigation, A.B. and G.G.; resources, M.P. and E.P.; data curation, M.P. and A.B.; writing—original draft preparation, A.B.; writing—review and editing, M.P., E.P. and G.G.; visualization, A.B. and E.P.; supervision, M.P.; project administration, M.P. and E.P.; funding acquisition, G.G. and M.P. All authors have read and agreed to the published version of the manuscript.

Funding: This research was funded by the Department of Civil, Environmental and Architectural Engineering (ICEA) of the University of Padova (project BIRD217038/21).

Institutional Review Board Statement: Not applicable.

Informed Consent Statement: Not applicable.

Data Availability Statement: The data presented in this study are available on request from the corresponding author. The data are not publicly available because they are a part of ongoing research.

Conflicts of Interest: The authors declare no conflict of interest.

References

1. Liu, Q.; Wu, J.; Qu, X.; Wang, C.; Oeser, M. Investigation of bitumen rheological properties measured at different rheometer gap sizes. *Constr. Build. Mater.* **2020**, *265*, 120287. [CrossRef]
2. Jing, R.; Varveri, A.; Liu, X.; Scarpas, A.; Erkens, S. Laboratory and field aging effect on bitumen chemistry and rheology in porous asphalt mixture. *Transp. Res. Rec.* **2019**, *2673*, 365–374. [CrossRef]

3. Jing, R.; Varveri, A.; Liu, X.; Scarpas, A.; Erkens, S. Rheological, fatigue and relaxation properties of aged bitumen. *Int. J. Pavement Eng.* **2019**, *21*, 1024–1033. [CrossRef]
4. Ishaq, M.A.; Giustozzi, F. Correlation between rheological tests on bitumen and asphalt low temperature cracking tests. *Constr. Build. Mater.* **2022**, *320*, 126109. [CrossRef]
5. Bueno, M.; García, A.; Partl, M.N. Application of strain-rate frequency superposition for bituminous binders. *Appl. Rheol.* **2015**, *25*, 65980.
6. Zhang, Z.; Fang, Y.; Yang, J.; Li, X. A comprehensive review of bio-oil, bio-binder and bio-asphalt materials: Their source, composition, preparation and performance. *J. Traffic Transp. Eng.* **2022**, *9*, 151–166. [CrossRef]
7. Porto, M.; Caputo, P.; Loise, V.; Abe, A.A.; Tarsi, G.; Sangiorgi, C.; Gallo, F.; Rossi, C.O. Preliminary study on new alternative binders through re-refined engine oil bottoms (REOBs) and industrial by-product additives. *Molecules* **2021**, *26*, 7269. [CrossRef]
8. Zhang, H.; Chen, Z.; Zhu, C.; Wei, C. An innovative and smart road construction material: Thermochromic asphalt binder. In *New Materials in Civil Engineering*; Samui, P., Kim, D., Iyer, N.R., Chaudhary, S., Eds.; Butterworth-Heinemann: Oxford, UK, 2020; pp. 691–716.
9. Zhang, Z.; Huang, Z.; Zhou, W.; Xu, R.; Xu, J.; Liu, Y. Study on synthesis and road performance of light-colored resin modified asphalt. *IOP Conf. Ser. Earth Environ. Sci.* **2021**, *770*, 012003. [CrossRef]
10. Iwański, M.; Mazurek, G. Rheological characteristics of synthetic wax-modified asphalt binders. *J. Chem. Technol. Polymer Proc.* **2012**, *57*, 661–664. [CrossRef]
11. Mullins, O.C.; Sheu, E.Y.; Hammami, A.; Marshall, A.G. *Asphaltenes, Heavy Oils, and Petroleomics*; Springer: Berlin, Germany, 2007.
12. Tang, P.; Mo, L.; Pan, C.; Fang, H.; Javilla, B.; Riara, M. Investigation of rheological properties of light colored synthetic asphalt binders containing different polymer modifiers. *Constr. Build. Mater.* **2018**, *161*, 175–185. [CrossRef]
13. Merusi, F.; Giuliani, F. Chromatic and rheological characteristics of clear road binders. *Transp. Res. Rec.* **2012**, *2293*, 114–122. [CrossRef]
14. Di Maria, V.; Rahman, M.; Collins, F.; Dondi, G.; Sangiorgi, C. Urban heat island effect: Thermal response from different types of exposed paved surfaces. *Int. J. Pavement Res. Technol.* **2013**, *6*, 414–422.
15. Pasetto, M.; Pasquini, E.; Giacomello, G.; Baliello, A. Innovative pavement surfaces as urban heat islands mitigation strategy: Chromatic, thermal and mechanical characterisation of clear/coloured mixtures. *Road Mat. Pav. Des.* **2019**, *20* (Suppl. 1), S533–S555. [CrossRef]
16. Navarro, F.J.; Partal, P.; Martínez-Boza, F.; Gallegos, C. Effect of composition and processing on the linear viscoelasticity of synthetic binders. *Eur. Polym. J.* **2005**, *41*, 1429–1438. [CrossRef]
17. Mansourkhaki, A.; Ameri, M.; Habibpour, M.; Underwood, B.S. Relations between colloidal indices and low-temperature properties of reclaimed binder modified with softer binder, oil-rejuvenator and polybutadiene rubber. *Constr. Build. Mater.* **2020**, *239*, 117800. [CrossRef]
18. Airey, G.D.; Rahimzadeh, B. Combined bituminous and mixture linear rheological properties. *Constr. Build. Mater.* **2004**, *18*, 535–548. [CrossRef]
19. Airey, G.D.; Mohammed, M.H.; Fichter, C. Rheological characteristics of synthetic road binders. *Fuel* **2008**, *87*, 1763–1775. [CrossRef]
20. Kriz, P.; Stastna, J.; Zanzotto, L. Temperature dependence and thermo-reversibility of physical hardening of asphalt binders. In Proceedings of the 4th Eurasphalt and Eurobitume Congress, Copenhagen, Denmark, 21–23 May 2008.
21. Divya, P.S.; Krishnan, J.M. How to consistently collect rheological data for bitumen in a dynamic shear rheometer? *SN Appl. Sci.* **2018**, *1*, 100. [CrossRef]
22. Grilli, A.; Bocci, M.; Virgili, A.; Conti, C. Mechanical characterization and chemical identification of clear binders for road surface courses. *Cold Tech. Mater. Sustain. Pavement Constr. Rehabil.* **2020**, *2020*, 4930646. [CrossRef]
23. Pasetto, M.; Baliello, A.; Giacomello, G.; Pasquini, E. Aesthetic and mechanical suitability of a clear synthetic resin as a unconventional binder for road pavements. *Adv. Mater. Sci. Eng.* **2019**, *2019*, 8643608. [CrossRef]
24. Sybilski, D.; Soenen, H.; Gajewski, M.; Chailleux, E.; Bankowski, W. Binder testing. In *Advances in Interlaboratory Testing and Evaluation of Bituminous Materials*; RILEM State-of-the-Art Report 9; Springer: Berlin, Germany, 2013.
25. Johnson, C.M.; Bahia, H.U.; Wen, H. Evaluation of strain-controlled asphalt binder fatigue testing in the dynamic shear rheometer. In Proceedings of the 4th International SIIV Congress, Palermo, Italy, 12–14 September 2007.
26. Williams, M.L.; Landel, R.F.; Ferry, J.D. The temperature dependence of relaxation mechanisms in amorphous polymers and other glass-forming liquids. *J. Am. Chem. Soc.* **1955**, *77*, 3701–3707. [CrossRef]
27. Bahia, H.U.; Hanson, D.I.; Zeng, M.; Zhai, H.; Khatri, M.A.; Anderson, R.M. Characterization of modified asphalt binders in Superpave mix design. In *NCHRP Report 459*; National Cooperative Highway Research Program: Washington, DC, USA, 2011.
28. Airey, G.; Sias, J.E.; Rowe, G.M.; Di Benedetto, H.; Sauzét, C.; Dave, E.V. An overview of Black space evaluation of performance and distress mechanisms in asphalt materials. In Proceedings of the RILEM International Symposium on Bituminous Materials, Lyon, France, 14–16 December 2020.
29. Little, D.N.; Allen, D.H.; Bashin, A. *Modeling and Design of Flexible Pavements and Materials*; Springer: Berlin, Germany, 2018.
30. Malkin, A.Y. Non-linearity in rheology—An essay of classification. *Rehol. Acta* **1995**, *34*, 27–39. [CrossRef]

31. Wyss, H.M.; Miyazaki, K.; Mattsson, J.; Hu, Z.; Reichman, D.R.; Weitz, D.A. Strain-rate frequency superposition: A rheological probe of structural relaxation in soft materials. *Phys. Rev. Lett.* **2007**, *98*, 238303. [CrossRef] [PubMed]
32. Fan, B.; Kazmer, D.O. Low-temperature modeling of the time-temperature shift factor for polycarbonate. *Adv. Polym. Technol.* **2005**, *24*, 278–287. [CrossRef]